Journal of Materials Chemistry A

Accepted Manuscript

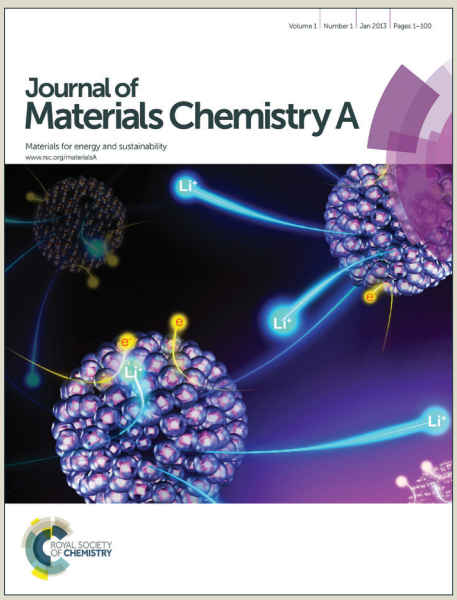

ROYAL SOCIETY OF CHEMISTRY

www.rsc.org/materialsA

Journal Name

RSCPublishing

ARTICLE

Hierarchical $NiCoO_2$ nanosheets supported on amorphous carbon nanotubes for high-capacity lithium-ion batteries with long cycle life

Cite this: DOI: 10.1039/xoxxoooooox

Received ooth January 2012,
Accepted ooth January 2012

DOI: 10.1039/xoxxoooooox

www.rsc.org/

Xin Xu, Bitao Dong, Shujiang Ding,* Chunhui Xiao and Demei Yu*

In this paper, we report a facile approach to synthesize one-dimension (1D) hierarchical $NiCoO_2$ nanosheets (NSs)@amorphous CNT composites based on the templates and carbon source of polymeric nanotubes (PNTs). Importantly, these sulfonated PNTs can be extended to prepare many other functional 1D metal oxides@amorphous CNT nanostructures, such as TiO_2, SnO_2, CoO and NiO, etc. Due to the outstanding nanostructures and the synergistic effects of the $NiCoO_2$ NSs and amorphous CNTs, an ultrahigh discharge capacity of 1309 mA h g^{-1} is delivered by the $NiCoO_2$@CNT composites even after 300 cycles at a current density of 400 mA g^{-1}. The favorable improvements of the $NiCoO_2$ based LIBs in this work illustrates that the 1D amorphous carbon matrix has significant effect for high-capacity metal oxide anode nanomaterials.

1. Introduction

In the last few decades, rechargeable lithium-ion batteries (LIBs) have become the dominant power source for portable electronic devices and electric vehicles.[1-3] On account of the low capacity and rate capability of the graphite (372 mA h g^{-1}), metal oxides have evolved as an important family of anode materials to be a high-capacity alternative.[4,5] In order to store and transport energy more efficiently, massive attention was focused on the choice of electrodes and design of metal oxides' structure. Ternary nickel cobaltite, a kind of typical ternary metal oxides, has been intensely investigated for supercapacitors and LIBs because of its low material cost, nontoxicity and environmentally friendly.[6,7] Due to the performance of transition metal oxides is highly depended on the micro-/nanostructures of the materials in various applications, so far, a series of versatile ternary nickel cobaltite nanostructures have been reported such as nanosheets,[8] nanoplates,[9] nanowires[10] and spheres.[11] In view of their smart nanosized architecture, the capacity of the LIBs has been impressively improved. Despite of the great progress, the cycling stability is still not very satisfactory for practical application due to the agglomeration and large volume change of the metal oxide nanostructures during the lithium ion charge–discharge process. In addition, most investigations have been focused on the spinel crystalline $NiCo_2O_4$, however, the other type of ternary nickel cobaltite $NiCoO_2$ has still rarely been studied especially in the field of LIBs. The Ni^{2+} could replace Co^{2+} in the NaCl-type crystal CoO structure and thus forming the cubic $NiCoO_2$.[12] Interestingly, some recent works reported that CoO based nanomaterials reveal preferable cycling stabilities.[13-15] On the basis of these results, it is attractive to investigate the electrochemical performance of the $NiCoO_2$ used as anode materials for LIBs.

Since the above-mentioned problems are difficult to be overcome only by designing the favorable nanostructures of the metal oxides, another effective approach is becoming urgent: fabricating hybrid nanostructures by embedding active metal oxide nanostructures into or immobilizing them onto a soft and conductive matrix (such as graphene and CNTs).[16-18] The highly flexible conductive matrix could not only buffer the large volume expansion and agglomeration of the active metal oxide nanostructures during the charge-discharge processes, but also enhance the electrical conductivity of the semiconducting materials. In addition, the 1D metal oxide-CNT composites' continuous framework and interconnected morphology can offer favorable pathways to facilitate the charge transfer. However, the production of common flexile conductive matrix such as CNTs and graphene ordinarily requires complex process control and high temperature, which limits their practical applications for LIBs on a large scale. Meanwhile, some amorphous carbon based hybrid materials prepared via relatively low temperature and facile route have obtained excellent electrochemical performance when they

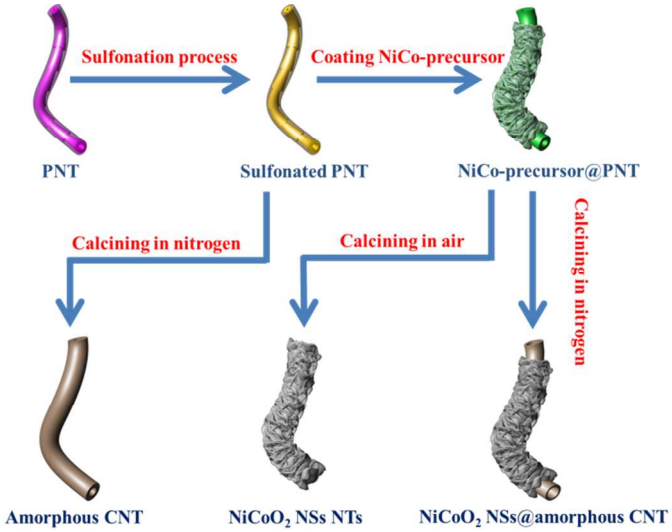

Scheme 1. Schematic illustration of the synthetic process of $NiCoO_2$ NSs@amorphous CNT composites, $NiCoO_2$ NSs NTs (nanotubes) and amorphous CNTs.

were evaluated as the anode materials of LIBs.[19-23] Compared to the common graphene and CNTs, the amorphous carbon possesses looser structure which may let it more effectively buffer the large volume change of the active metal oxide nanostructures during the fast charging–discharging process. Therefore, the low-cost amorphous carbon could not only enhance the cycling stability of the metal oxide nanostructures, but also make it possible to prepare the metal oxides-carbon based nanomaterials on a large scale for commercial LIBs.

In this paper, we describe a novel strategy to fabricate 1D $NiCoO_2$ nanosheets (NSs)@amorphous CNT composites by using polymeric nanotubes (PNTs) with uniform size as hard templates and carbon source, which are synthesized by cationic polymerization of divinylbenzene using immiscible initiator nanodroplets of boron trifluoride etherate complex and followed a sulfonation process.[24] These sulfonated PNTs can not only induce a favorable adsorption of the metal ions precursors to form various 1D morphology, but also provide a low-cost and facile route to obtain the amorphous CNTs conductive matrix after a low-temperature calcination process, which could make it possible to prepare the $NiCoO_2$@CNT composites on a large scale for commercial LIBs.[25-27] Scheme 1 shows the synthetic process of the $NiCoO_2$ NSs@amorphous CNT composites. Firstly, we prefabricate NiCo-precursor@PNT coaxial nanocables based on in situ growth of NiCo-precursor ultrathin NSs from the sulfonated gel matrix of sulfonated PNTs. After being calcined in nitrogen, the sulfonated PNTs are carbonized to be amorphous CNTs core[27] and the NiCo-precursor NSs are totally transformed to highly crystallized $NiCoO_2$ shell. Finally, the amorphous CNTs covered with well-developed hierarchical $NiCoO_2$ NSs are successfully obtained, which delivers good cycling stability and excellent rate capability, thus exhibiting great potential as an anode material for lithium storage. In addition, this facile and generic solution method to fabricate 1D metal oxides@amorphous CNT nanostructures is expected to have wide range of applications in improving the properties of other traditional metal oxides (such as TiO_2, SnO_2, CoO and NiO, etc).

2. Experimental Section

2.1 Material Synthesis

Sulfonated PNTs: PNTs were prepared according to a previously reported method.[24] PNTs (3 g) were added to concentrated sulfuric acid (PNTs: H_2SO_4 = 1: 30, w/w) and the mixture was ultrasonicated for 10 min to ensure well dispersion. After being stirred for 24 h at 40 °C, the pink precipitate was collected by centrifugation and washed with ethanol.[28-30]

NiCo-precursor@PNT: 375 mg $Ni(NO_3)_2{\cdot}6H_2O$, 375 mg $Co(NO_3)_2{\cdot}6H_2O$ and 175 mg hexamethylenetetramine (HMT) were dissolved into 200 mL 0.7 mM trisodium citrate solution. Then 50 mg sulfonated PNTs were dispersed into the above solution by sonication for 30 minutes. The reaction mixture was then transferred into a 500 mL round bottom flask. After stirring for 6 h at 90 °C, the flask was left to cool down to room temperature. The green precipitate was collected by centrifugation, washed thoroughly with ethanol, and dried at 60 °C overnight.

$NiCoO_2$ NSs@amorphous CNT composites and pure $NiCoO_2$ NSs NTs: the as-prepared NiCo-precursor@PNT composite was calcined at 500 °C for 4 h with a heating rate of 1 °C min^{-1} in nitrogen and air, respectively (Scheme 1).

Amorphous CNTs: The sulfonated PNTs were also carbonized in nitrogen for 4 h at 500 °C with a heating rate of 1 °C min^{-1} to obtain the amorphous CNTs (Scheme 1).

2.2 Characterization

The product morphology was examined using field-emission scanning electron microscopy (FESEM; JEOL, JSM-7000F) and transmission electron microscopy (TEM; JEOL, JEM-2100). The Raman spectra was performed on a Raman spectrometer under a backscattering geometry (λ=514nm; HORIBA JOBIN YVON, HR 800). The specific surface area and pore size distribution of the products were measured using a BET analyzer (Autosorb-iQ, Quantachrome Instruments U.S.) at 77 K. The crystallographic information of the samples was collected using powder X-ray diffraction (XRD; SHIMADZU, Lab X XRD-6000). The thermogravimetric analysis (METTLER-TOLEDO TGA 1) was carried out under a flow of air with a temperature ramp of 10 °C/min from room temperature to 450 °C.

2.3 Electrochemical measurements

The electrochemical tests were performed under ambient temperature using two-electrode coin cells (CR 2016) with lithium serving as both the counter electrode and the reference electrode. The working electrode consisted of active materials ($NiCoO_2$@CNT composites, $NiCoO_2$ NSs NTs, amorphous CNTs), conductive agent (carbon black, C-NERGY™ Super

C65), and polymer binder (poly(vinylidenedifluoride), PVDF, Aldrich) in a 70: 20: 10 weight ratio. The electrolyte used was 1.0 M LiPF6 in a 50: 50 (w/w) mixture of ethylene carbonate and diethyl carbonate. Cell assembly was carried out in an Ar-filled glovebox with concentrations of moisture and oxygen below 1.0 ppm. Cyclic voltammetry was performed using an electrochemical workstation (CHI 660D). The charge–discharge tests were performed using a NEWARE battery tester.

3. Results and discussion

Fig. 1 shows the typical morphology of the sulfonated PNT templates and NiCo-precursor@PNT composite. The field-emission scanning electron microscope (FESEM) image of sulfonated PNT templates indicates the large-scale and uniform features of the products (Fig. 1A), and the bamboo-like tubular structure and smooth surface can be clearly observed from the transmission electron microscope (TEM) image (Fig. 1B). Fig. 1C shows that almost every PNT is covered with the NiCo-precursor ultrathin NSs, which is attributed to the large amount of functional groups ($–SO_3$) uniformly distributed on the surface of the PNTs together with the assist function of the hexamethylenetetramine and trisodium citrate. A further TEM observation demonstrates the uniform growth of hierarchical and standing NiCo-precursor nanostructures surrounding the PNT backbone to form the 1D architecture (Fig. 1D).

After annealing in nitrogen, the NiCo-precursor NSs can be converted to crystallized $NiCoO_2$ and the PNTs templates are totally carbonized to be amorphous CNTs. As shown in Fig. 2A and B, the $NiCoO_2$@CNT composites maintain the tubular and hierarchical structures, which reveal the excellent structure stability of these samples. From Fig. 2C, it can be observed that the as-obtained $NiCoO_2$ NSs are slightly shrinking compared with the NiCo-precursor NSs on account of the thermal conversion. Moreover, as shown in Fig. 2D, the $NiCoO_2$ NSs are consist of small nanoparticles and the porous feature of the products can be exhibited. Such hierarchical and porous nanostructures could provide extra space to store more lithium ions, suppress their large volume change and decrease the lithium ions' diffusion length, which are beneficial for the cycling stability of anode materials. Importantly, the successful growth of high-quality $NiCoO_2$ NSs on the amorphous CNT is very important for the fabrication of so-called wearable, light-weight or flexible energy-storage devices, which will find broad applications in many situations.[8] The HRTEM image (Fig. 2E) taken from the $NiCoO_2$ NSs shows the obvious crystalline lattice with interplane spacing of 0.24 nm, corresponding to the (111) plane of cubic $NiCoO_2$ phase. The selected-area electron diffraction (SAED) pattern (Fig. 2F) exhibits five intense rings indexed to the (111), (200), (220), (311), (222) planes of $NiCoO_2$ NSs, which is consistent with the XRD results lately described.

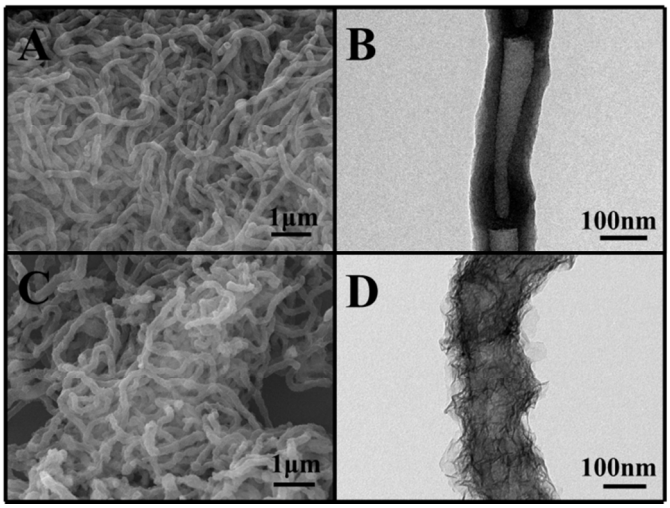

Fig. 1 (A) SEM image and (B) TEM image of sulfonated PNT templates; (C) SEM image and (D) TEM image of NiCo-precursor NSs@PNT composites.

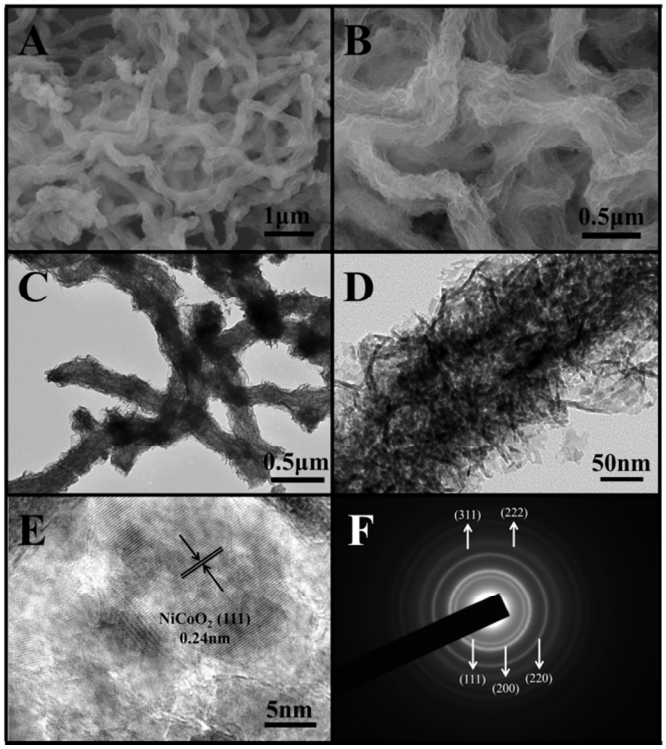

Fig. 2 SEM (A, B) images, TEM (C, D) images, HRTEM image (E) and SAED pattern (F) of $NiCoO_2$ NSs@amorphous CNT composites.

The porous characteristic of the $NiCoO_2$ NSs@amorphous CNT composites is also studied by the the nitrogen adsorption/desorption isotherm and pore-size distribution curve (Fig. 3A). It is worth noting that the Brunauer–Emmett–Teller (BET) specific surface area of these products is calculated to be 200 $m^2 g^{-1}$, which is much larger than the previously reported porous $NiCo_2O_4$ nanomaterials.[8,11,31-33] This is probably due to the amorphous CNTs obtained from carbonizing the PNTs also contribute a high specific surface area.[27] It can also be observed that the size of the most mesopores is about 4 nm which are corresponding to the aggregation of $NiCoO_2$ nanoparticles within the sheet-like subunits.

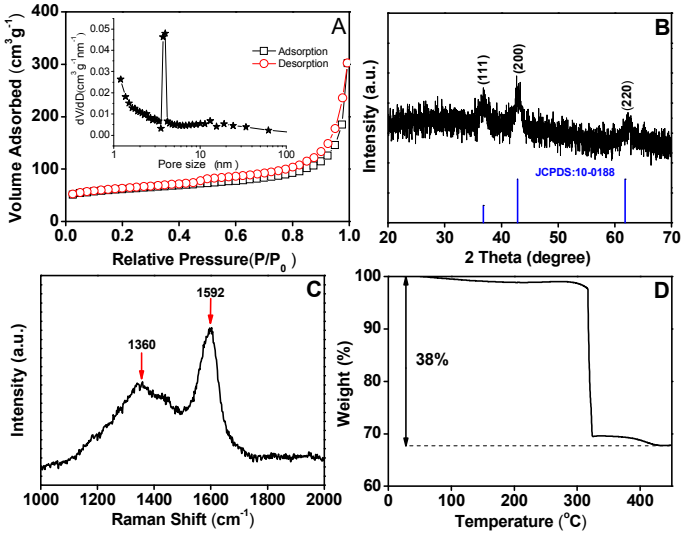

Fig. 3 (A) N_2 adsorption–desorption isotherms of the $NiCoO_2$@CNT composites, the inset shows the pore-size distribution calculated from the desorption branch; (B) XRD patterns, (C) Raman spectra and (D) TGA curve of $NiCoO_2$@CNT composites.

Fig. 3B shows the corresponding XRD pattern of the $NiCoO_2$ NSs@amorphous CNT composites. As can be seen, all the peaks of the annealed sample can be unambiguously assigned to the cubic $NiCoO_2$ phase (JCPDS card no. 10-0188).

Raman spectroscopy is proven to be necessary to characterize carbon in composite materials.[34] As shown in Fig. 3C, a couple of peaks (~1360 and 1592 cm^{-1}) in the wavenumber range of 1000–2000 cm^{-1} can be clearly observed, which are attributed to the A_{1g} vibration mode of the disordered carbon (D-band) and the E_{2g} vibration mode of the ordered graphitic carbon (G-band), respectively. It confirms that the carbon in the composite is amorphous carbon. Fig. 3D shows the thermal behavior of the $NiCoO_2$@CNT composites studied by TGA under air atmosphere. The samples show a significant weight loss at about 320 °C, which can be ascribed to the decomposition of the amorphous CNTs. After reaching 500 °C, the $NiCoO_2$@CNT composites show a total weight loss of 32.0%, and the weight fraction of $NiCoO_2$ NSs in the as-prepared $NiCoO_2$@CNT composites is calculated to be 68.0%.

We subsequently investigate the electrochemical properties of these $NiCoO_2$ NSs@amorphous CNT composites as anode materials for LIBs. Fig. 4A shows the cyclic voltammograms (CVs) of $NiCoO_2$@CNT composites for the first, second and fifth cycles at a scan rate of 0.5 mV s^{-1} over a voltage range of 0.01-3.00 V versus Li/Li$^+$. For the first cathodic scan, there is an intense peak located around 0.45 V which can be ascribed to the reduction of Ni^{2+} and Co^{2+} to metallic Ni and Co, respectively. During the following anodic sweep, the two peaks at around 1.65 V and 2.27 V could be attributed to the oxidation of Ni^0 to Ni^{2+} and Co^0 to Co^{2+}. In the subsequent cycles, the reduction peak becomes weak and shifts to ca. 0.85 V and there is no significant change in the potentials of the oxidation peaks at ca. 1.65 V and 2.27 V.[9,11,32,35,36] On the basis of the cyclic

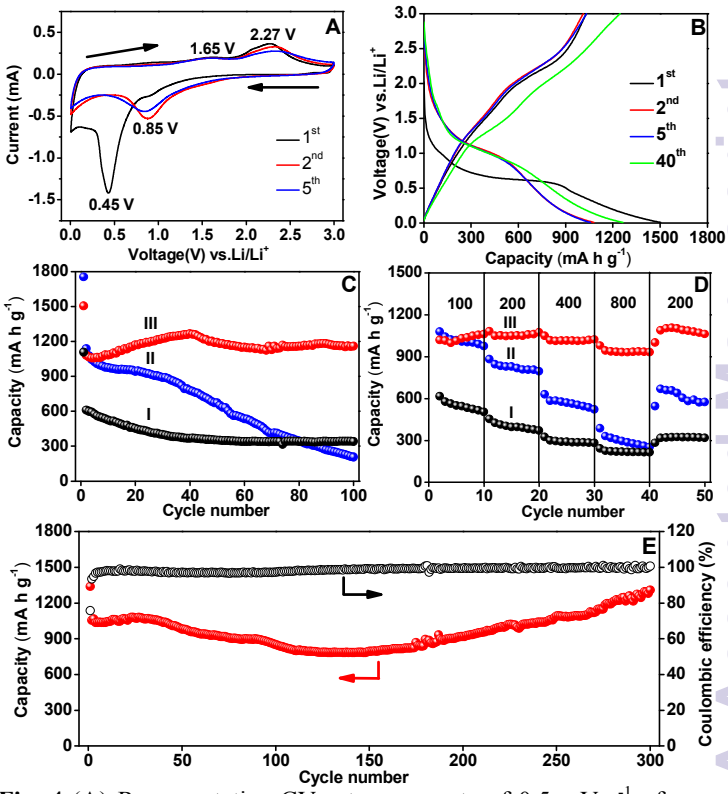

Fig. 4 (A) Representative CVs at a scan rate of 0.5 mV s^{-1} of $NiCoO_2$@CNT composites; (B) charge–discharge voltage profiles at a current density of 200 mA g^{-1} of $NiCoO_2$@CNT composites; (C) comparative cycling performance of amorphous CNTs (I), $NiCoO_2$ NSs NTs (II) and $NiCoO_2$@CNT composites (III) at a current density of 200 mA g^{-1}. (D) Cycling performance of amorphous CNTs (I), $NiCoO_2$ NSs NTs (II) and $NiCoO_2$@CNT composites (III) at different current densities indicated (mA g^{-1}). (E) Cycling performance and corresponding Coulombic efficiency of $NiCoO_2$@CNT composites at a current density of 400 mA g^{-1}.

voltammograms tests together with the storage mechanisms of NiO and CoO reported previously, the whole electrochemical process are believed to proceed as follows:

$$NiCoO_2 + 4Li^+ + 4e^- \rightarrow Ni + Co + 2Li_2O$$

$$Ni + Li_2O \leftrightarrow NiO + 2Li^+ + 2e^-$$

$$Co + Li_2O \leftrightarrow CoO + 2Li^+ + 2e^-$$

Fig. 4B shows the charge–discharge voltage profiles of the $NiCoO_2$@CNT composites for the first, second, fifth and fortieth cycles at a current density of 200 mA g^{-1}. As can be seen, there are two plateaus around 1.6 and 2.3 V in the charge process, which are in agreement with the anode peaks in the CV. There is one plateau in the discharge process, demonstrating the reduced reaction of Ni^{2+} and Co^{2+}. In addition, it is also observed that the first discharge/charge capacities are 1504 and 1031 mA h g^{-1}, indicating the irreversible capacity loss of about 31%, which is common to NiO and CoO based electrode materials. Fig. 4c gives the cycling performance of the

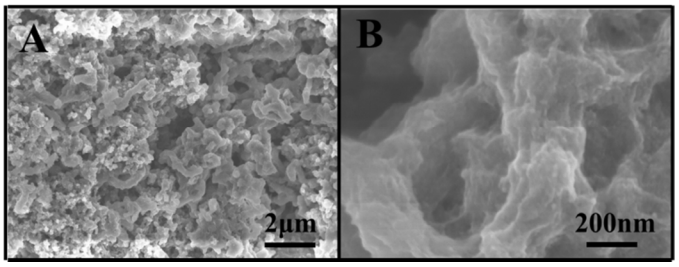

Fig. 5 SEM (A, B) images of the $NiCoO_2$@CNT composites electrode after 6 cycles at a current density of 400 mA g^{-1}.

$NiCoO_2$@CNT composites, pure $NiCoO_2$ NSs NTs and as-prepared amorphous CNTs at the same current density of 200 mA g^{-1}. As can be seen, the initial discharge capacity of the pure $NiCoO_2$ NSs NTs (1753 mA h g^{-1}) is higher than the $NiCoO_2$@CNT composites, which is attributed to the existence of amorphous CNTs in the hybrid materials. During the first forty cycles, the discharge capacities of the pure $NiCoO_2$ NSs NTs show a relatively slower decrease, which is profit from their hierarchical and mesoporous nanostructures. Oppositely, the reversible capacities of the $NiCoO_2$@CNT composites show an interesting upward trend. This phenomenon can be ascribed to the synergistic effect between the $NiCoO_2$ NSs and amorphous CNTs,[16] and the growth of the gel-like polymeric layer and possibly electrochemical activation of the hybrid composites during the cycling process.[37-44] After the 40th cycle, the discharge capacities of the $NiCoO_2$ NSs NTs reveal a rapidly decrease until below the specific capacity of amorphous CNTs, indicating the unavoidable breakdown of the $NiCoO_2$ nanostructures. However, after a slight decrease, the cycling performance of the $NiCoO_2$@CNT composites become extremely stable, which highly proved the significance of the synergistic effect provided by amorphous CNTs once again. Furthermore, the excellent cycling stability of $NiCoO_2$@CNT composites is also superior to most reported $NiCo_2O_4$ based materials.[9,11,45] Fig. 4D illustrates the current density dependence of the discharge capacity of the $NiCoO_2$@CNT composites, bare $NiCoO_2$ NSs NTs and amorphous CNTs. At different current densities of 100, 200, 400 and 800 mA g^{-1}, the capacities of $NiCoO_2$@CNT composites are 1061, 1074, 1024 and 933 mA h g^{-1}, respectively. When the current density return to 200 mA g^{-1}, the $NiCoO_2$@CNT composites still deliver a capacity of 1063 mA h g^{-1}, almost no capacity loss after 50 cycles. Similar to the cycling performances, the $NiCoO_2$ NSs NTs and amorphous CNTs still display inferior rate capabilities compared with the $NiCoO_2$@CNT composites. To further determine the superiority of the $NiCoO_2$@CNT composites, we subsequently investigate their cycling performance with a long cycle life at a higher current density of 400 mA g^{-1}. As one can see from Fig. 4E, although experiencing a slow decrease during the first half of cycling on account of the unavoidable breakdown of the $NiCoO_2$ nanostructures, there is almost no capacity loss compared with their initial reversible capacity even after prolonged cycling over 300 cycles, which can be explained by the growth of the gel-like polymeric layer and possibly electrochemical activation of the hybrid composites during the cycling process.[37-44] The reasons for the excellent lithium storage performance of the $NiCoO_2$@CNT composites could be explained as follows: i) the ternary metal oxides $NiCoO_2$ possesses much better electrical conductivity and higher redox activity compared to the single constituents such as NiO and CoO;[7,8,10] ii) the hierarchical $NiCoO_2$ NSs possess higher specific surface area which can provide more sites for lithium ions storage; iii) massive void spaces derived from cavity and piling up $NiCoO_2$ NSs could effectively buffer the strain generated during the fast charging–discharging process; iv) the inside amorphous CNTs could enhance the electrical conductivity, relieve the aggregation and buffer the large volume change of the $NiCoO_2$ NSs, thus obtain the so-called synergistic effects; v) the continuous 1D morphology of the $NiCoO_2$@CNT composites can stack into non-woven fabrics like networks to provide more paths for lithium ions' transport.

Fig. 5 shows the morphology of $NiCoO_2$@CNT composites electrode after 6 cycles at a current density of 400 mA g^{-1} to further understand the excellent electrochemical performance of products. After the charge-discharge cycles, the $NiCoO_2$@CNT composites still remain their 1D tubular structures (Fig. 5A), suggesting their high stability. In addition, the hierarchical $NiCoO_2$ NSs can also be observed from Fig. 5B, indicating they are beneficial to relax the volume expansion and alleviate the structure damage during the charge-discharge processes.

Conclusions

In summary, a kind of 1D hierarchical $NiCoO_2$ NSs@amorphous CNT composites was successfully synthesized as a high-performance anode material for LIBs. The as-prepared products exhibited extremely high discharge capacity of 1309 mA h g^{-1} at a current density of 400 mA g^{-1} even after 300 cycles and lead to no capacity loss, due to the smart architecture of the $NiCoO_2$@CNT composites and the favorable synergistic effect between the $NiCoO_2$ NSs and amorphous CNTs. More importantly, the amorphous CNT obtained from the low-cost and easy-to-make sulfonated PNTs provided an outstanding improvement for the electrochemical performance of the metal oxides nanostructures, which presents potential applications in large-scale energy storage systems.

Acknowledgements

This research was supported partially by the National Natural Science Foundation of China (No. 51273158, 21303131); Natural Science Basis Research Plan in Shaanxi Province of China (No. 2012JQ6003, 2013KJXX-49); Ph.D. Programs Foundation of Ministry of Education of China (No. 20120201120048); Program for New Century Excellent Talents in University (NCET-13-0449). The authors are grateful to the Fundamental Research Funds for the Central Universities for financial support.

Notes and references

State Key Laboratory for Mechanical Behavior of Materials and MOE Key Laboratory for Nonequilibrium Synthesis and Modulation of Condensed Matter and Department of Applied Chemistry, School of Science, Xi'an Jiaotong University, Xi'an 710049, China.

1 J. M. Tarascon and M. Armand, *Nature*, 2001, **414**, 359.
2 P. Simon and Y. Gogotsi, *Nat. Mater.*, 2008, **7**, 845.
3 J. B. Goodenough and Y. Kim, *Chem. Mater.*, 2010, **22**, 587.
4 X. M. Sun, J. F. Liu and Y. D. Li. *Chem. Mater.*, 2006, **18**, 3486.
5 X. W. Lou, C. M. Li and L. A. Archer, *Adv. Mater.*, 2009, **21**, 2536.
6 B. Cui, H. Lin, J. B. Li, X. Li, J. Yang and J. Tao, *Adv. Funct. Mater.*, 2008, **18**, 1440.
7 T. Y. Wei, C. H. Chen, H. C. Chien, S. Y. Lu and C. C. Hu, *Adv. Mater.*, 2010, **22**, 347.
8 G. Q. Zhang and X. W. Lou, *Adv. Mater.*, 2013, **25**, 976.
9 Y. J. Chen, M. Zhuo, J. W. Deng, Z. Xu, Q. H. Li and T. H. Wang, *J. Mater. Chem. A*, 2014, **2**, 4449.
10 H. Jiang, J. Ma and C. Z. Li, *Chem. Commun.*, 2012, **48**, 4465.
11 J. F. Li, S. L. Xiong, Y. R. Liu, Z. C. Ju and Y. T. Qian, *ACS Appl. Mater. Interfaces*, 2013, **5**, 981.
12 J. W. Xiao and S. H. Yang, *J. Mater. Chem.*, 2012, **22**, 12253.
13 J. H. Kim and Y. C. Kang, *Nanoscale*, 2014, **6**, 4789.
14 D. D. Li, L. X. Ding, S. Q. Wang, D. D. Cai and H. H. Wang, *J. Mater. Chem. A*, 2014, **2**, 5625.
15 M. Zhang, E. Uchaker, S. Hu, Q. F. Zhang, T. H. Wang, G. Z. Cao and J. Y. Li, *Nanoscale*, 2013, **5**, 12342.
16 G. M. Zhou, D. W. Wang, L. C. Yin, N. Li, F. Li, and H. M. Cheng, *ACS Nano*, 2012, **6**, 3214.
17 D. N. Wang, J. L. Yang, X. F. Li, D. S. Geng, R. Y. Li, M. Cai, T. K. Sham and X. L. Sun, *Energy Environ. Sci.*, 2013, **6**, 2900.
18 X. Li, X. Meng, J. Liu, D. Geng, Y. Zhang, M. Banis, Y. Li, R. Li, X. Sun, M. Cai and M. Verbrugge, *Adv. Funct. Mater.*, 2012, **22**, 1647.
19 X. G. Liu, S. W. Or, C. G. Jin, Y. H. Lv, C. Feng and Y. P. Sun, *Carbon*, 2013, **60**, 215.
20 Y. Wang, M. H. Wu, Z. Jiao and J. Y. Lee, *Chem. Mater.*, 2009, **21**, 3210.
21 M. F. Hassan, M. M. Rahman, Z. P. Guo, Z. X. Chen and H. K. Liu, *J. Mater. Chem.*, 2010, **20**, 9707.
22 Y. M. Chen, Z. G. Lu, L. M. Zhou, Y. W. Maia and H. T. Huang, *Energy Environ. Sci.*, 2012, **5**, 7898.
23 G. Q. Zhang, H. B. Wu, H. E. Hostera and X. W. Lou, *Energy Environ. Sci.*, 2014, **7**, 302.
24 W. Ni, F. X. Liang, J. G. Liu, X. Z. Qu, C. L. Zhang, J. L. Li, Q. A. Wang and Z. Z. Yang, *Chem. Commun.*, 2011, **47**, 4727.
25 Z. Z. Yang, Z. W. Niu, Y. F. Lu, Z. B. Hu and C. C. Han, *Angew. Chem. Int. Ed.*, 2003, **42**, 1943.
26 M. Yang, J. Ma, C. L. Zhang, Z. Z. Yang and Y. F. Lu, *Angew. Chem. Int. Ed.*, 2005, **44**, 6727.
27 H. J. Zhou, L. Liu, X. C. Wang, F. X. Liang, S. J. Bao, D. M. Lv, Y. K. Tang and D. Z. Jia, *J. Mater. Chem. A*, 2013, **1**, 8525.
28 X. Xu, J. Liang, H. Zhou, D. M. Lv, F. X. Liang, Z. L. Yang, S. J. Ding and D. M. Yu, *J. Mater. Chem. A*, 2013, **1**, 2995.
29 X. Xu, G. R. Yang, J. Liang, S. J. Ding, C. L. Tang, H. H. Yang, W. Yan, G. D. Yang and D. M. Yu, *J. Mater. Chem. A*, 2014, **2**, 116.
30 S. J. Ding, J. S. Chen and X. W. Lou, *Adv. Funct. Mater.*, 2011, **21**, 4120.
31 H. B. Wu, H. Pang and X. W. Lou, *Energy Environ. Sci.*, 2013, **6**, 3619.
32 L. L. Li, Y. L. Cheah, Y. Ko, P. Teh, G. Wee, C. L. Wong, S. J. Peng and M. Srinivasan, *J. Mater. Chem. A, 2013*, 1, 10935.
33 L. Qian, L. Gu, L. Yang, H. Y. Yuan and D. Xiao, *Nanoscale*, 2013, 5, 7388.
34 Y. Xia, W. K. Zhang, Z. Xiao, H. Huang, H. J. Zeng, X. R. Chen, F. Chen, Y. P. Gan and X. Y. Tao, *J. Mater. Chem.*, 2012, **22**, 9209.
35 X. H. Wang, L. Qiao, X. L. Sun, X. W. Li, D. K. Hu, Q. Zhang and D. Y. He, *J. Mater. Chem. A*, 2013, **1**, 4173.
36 X. H. Wang, Y. Fan, R. A. Susantyoko, Q. Z. Xiao, L. M. Sun, D. Y. He, Q. Zhang, *Nano Energy*, 2014, **5**, 91.
37 G. Q. Zhang, L. Yu, H. B. Wu, H. E. Hoster, and X. W. Lou, *Adv. Mater.*, 2012, **24**, 4609.
38 X. S. Zhou, L. J. Wan and Y. G. Guo, *Chem. Commun.*, 2013, **49**, 1838.
39 Z. S. Wu, Y. Sun, Y. Z. Tan, S. Yang, X. Feng and K. Müllen, *J. Am. Chem. Soc.*, 2012, **134**, 19532.
40 Z. Y. Wang, D. Y. Luan, S. Madhavi, Y. Hu and X. W. Lou, *Energy Environ. Sci.*, 2012, **5**, 5252.
41 W. Wei, S. B. Yang, H. X. Zhou, I. Lieberwirth and X. L. Feng *and* K. Müllen, *Adv. Mater.*, 2013, **25**, 2909.
42 D. N. Wang, J. L. Yang, X. F. Li, D. S. Geng, R. Li, M. Cai, T. K. Sham and X. L. Sun, *Energy Environ. Sci.*, 2013, **6**, 2900.
43 X. H. Wang, X. W. Li, X. L. Sun, F. Li, Q. M. Liu, Q. Wang and D. Y. He, *J. Mater. Chem.*, 2011, **21**, 3571.
44 X. H. Wang, Z. B. Yang, X. L. Sun, X. W. Li, D. S. Wang, P. Wang and D. Y. He, *J. Mater. Chem.*, 2011, **21**, 9988.
45 Y. NuLi, P. Zhang, Z. P. Guo, H. K. Liu, and J. Yanga, *Electrochem. Solid-State Lett.*, 2008, **11**, A64.

Graphical Abstract

$NiCoO_2$ nanosheets@amorphous CNT composites show enhanced cycling performance and rate capability as anode materials for lithium-ion batteries.